Materials Science in Semiconductor Processing 83 (2018) 42–49

Contents lists available at ScienceDirect

Materials Science in Semiconductor Processing

journal homepage: www.elsevier.com/locate/mssp

Structure, optical, electrical and thermoelectric properties of solution-processed Li-doped NiO films grown by SILAR

N.P. Klochko[a], K.S. Klepikova[a,*], D.O. Zhadan[a], S.I. Petrushenko[b], V.R. Kopach[a], G.S. Khrypunov[a], V.M. Lyubov[a], S.V. Dukarov[b], V.O. Nikitin[a], M.O. Maslak[a], A.Yu. Zakovorotniy[a], A.L. Khrypunova[a]

[a] National Technical University "Kharkiv Polytechnic Institute", 2, Kyrpychova str., 61002 Kharkiv, Ukraine
[b] V.N. Karazin Kharkiv National University, 4, Svobody Square, 61000 Kharkiv, Ukraine

ARTICLE INFO

Keywords:
Li-doped NiO
SILAR
Thermoelectric
Resistivity
Crystal structure
Optical property

ABSTRACT

The article presents a new facial synthesis of Li-doped NiO films (NiO:Li) via an easy and cost-effective method Successive Ionic Layer Adsorption and Reaction (SILAR) with the processing of the obtained NiO films in a lithium-containing aqueous solution for their transformation after annealing into NiO:Li layers. Comparative analysis of crystal structure, optical, electrical and thermoelectric properties of the obtained NiO and NiO:Li 420-1050 nm thick films have reveiled a cubic rock-salt NiO structure, at that, NiO:Li samples are nanocrystalline single phased Li-NiO solid solutions. The fabricated NiO and NiO:Li films are *p*-type semiconductors with activation energy E_a = 0.1 eV and E_a = 0.25–0.31 eV, respectively. The obtained in-plane Seebeck coefficients Z are in the range 0.20–0.33 mV/K. Notwithstanding the fact that the maximum values of the thermoelectric power factors P = 2.2 μW/K^2·m, are rather small, they were achieved if the hot end of the NiO:Li film was heated only to 115 °C. Thus, the produced in this work new low cost thermoelectric thin film material is suitable for a production of electrical energy for low-power devices due to absorption of low-potential heat.

1. Introduction

Thermoelectric technology which provides direct conversion of heat into electricity has made enormous progress as a viable alternative for certain power generating applications due to the urgency of our energy and environmental issues [1–7]. Especially great efforts of advanced nanoscience and nanotechnology are aimed at creating of microscale, wearable and implantable thermoelectric generators (TEGs) used to produce electrical power for devices, such as wireless sensors, requiring micro-Watts to milli-Watts of power per device [1–7]. These TEGs collect low thermal energy from sun light, waste heat sources or from human bodies, which have temperature differences or spatial dimensions that are too small for conventional thermodynamic heat engines to effectively utilize heat energy. Substantial numbers of modern researches focus on the creation of new thin-film non-poisonous, earth-abundant, low cost and stable thermoelectric materials that can effectively utilize low temperature heat [3–7]. Among them wide bandgap inorganic semiconductor nickel oxide (NiO) is available, stable, inexpensive material with excellent structural, optical, magnetic and electrical properties, which can be manufactured using various methods. Therefore, NiO thin films are of great interest in a wide range of applications like electrochromic devices, smart windows, gas sensors, semi-transparent diodes, fuel cells and thermoelectric generators [8–16]. The problem for the use of nickel oxide in many of the applications listed above is its rather small electrical conductivity, especially at near room temperatures [11,13,16–24]. According to [16,20,21,23,24], stoichiometric NiO is an insulator with a resistivity (ρ) of 10^{11} Ω m at room temperature, but its ρ can be decreased by increasing the concentration of Ni^{3+} ions, which results from the introduction of nickel vacancies and interstitial oxygen atoms, thus, nickel oxide is common known as a *p*-type semiconductor. An additional reduction of the NiO resistance is ensured by its doping with La [18], Na [17] and Li [11,13,16,17,19–24]. As reported in [20], the substitution of Li^+ for Ni^{2+} in the Li-doped NiO (NiO:Li) can increase the concentrations and mobility of the carriers (holes) together with decreasing thermal conductivity of the material, because Li doping can enhance the scattering of phonons. As a result of the increase of electrical conductivity and reduction of thermal conductivity, Li doping can enhance the thermoelectric figure of merit of NiO:Li material to be used in high-performance thermoelectric devices [11,13,16,17,19–24]. Earlier studies [22,23] showed an efficiency of NiO:Li in thermoelectric hydrogen sensors at the operating temperatures in the 140–180 °C

* Correspondence to: Department of Materials for electronics and solar cells, National Technical University "Kharkiv Polytechnic Institute", 2, Kyrpychova str., 61002 Kharkiv, Ukraine.
E-mail address: catherinakle@gmail.com (K.S. Klepikova).

https://doi.org/10.1016/j.mssp.2018.04.010
Received 26 February 2018; Received in revised form 2 April 2018; Accepted 9 April 2018

range. This gives us hope for the possibility of creating microscale TEGs with micro-Watts electrical power output at temperature differences of several tens of Kelvins, which can operate using NiO:Li thin films as *p*-thermolegs at near room temperatures.

Currently, the most of the NiO:Li thermoelectric materials are ceramics fabricated by sintering the mixed reactant powders [17,19,20,22]. The methods available for the fabrication of NiO and NiO:Li thin-films suitable for the microscale thermoelectric devices usually need special equipment and the processes are time consuming such as pulsed laser deposition [24], electron beam evaporation of Ni films and their conversion into NiO thin films by air atmosphere annealing [14], and magnetron sputtering [10,16]. Note, that the magnetron sputtered in [10] NiO thin films demonstrate high ρ, and magnetron sputtered by authors [16] NiO:Li thin films have unstable electrical properties. Another approach is the deposition of Li-doped NiO thin films with rather high resistivity via sol–gel method ($\rho > 10;\Omega$ m in [21]; $\rho > 10^2$ Ω m in [23]). Recently, nanocrystalline NiO thin films were synthesized using a low temperature solution growth by means of Successive Ionic Layer Adsorption and Reaction (SILAR) technique [15,25,26]. Compared to the above-mentioned methods, SILAR is facile, low cost, affordable and suitable for mass production approach for the layer-by-layer growing of chemically stable semiconductor NiO films with good control over the deposition process and film thickness. As-prepared via SILAR NiO films [26] (or Ni $(OH)_2$ films, according to the [15,25,27]) have rather high resistivity ($\rho \approx$ 1–8 Ω m at 300 K [26]). For the improvement of the crystal structure and lowering the resistivity, the as-deposited samples must be annealed at 575 °C for 2 h [25] or at 573 K for 1 h [15] in air ambient in order to form NiO, which was qualitatively confirmed as the surface appearance was changed from faint greenish to dark black [15]. However, as shown in [15], nickel oxide films after their annealing suffer from deep fissures, which make them unsuitable for thermoelectrical energy conversion. Therefore, we were unable to find in the literature any information about the use of SILAR for the creation of NiO films for TEGs. Also, it was not possible to receive data on the production of lithium-doped nickel oxide films by using SILAR method.

The proposed article presents a new facial synthesis of Li-doped NiO films via an easy and cost-effective method SILAR with the processing of the obtained films in a lithium-containing aqueous solution for their transformation after annealing into conductive NiO:Li layers. Here we demonstrate also the results of the research of structure, optical, electrical and thermoelectric properties of these solution-processed Li-doped NiO films grown by SILAR.

2. Experimental details

In this study, NiO and NiO:Li thin films were synthesized by means SILAR method on glass substrates. Aqueous nickel-ammonia complex ions ($[Ni(NH_3)_4]^{2+}$) were chosen as the basis of a cationic precursor, which solution contained 0.1 M $NiCl_2$, and pH value was adjusted to ~11.5 by adding aqueous ammonia. For the synthesis of the NiO and NiO:Li thin films, one SILAR growth cycle included following four steps: (1) immersing the substrate into cationic precursor solution for 30 s to create a thin liquid film containing $[Ni(NH_3)_4]^{2+}$ complex cation on the substrate; (2) immersing this substrate immediately into hot water (90 °C) for 7 s to form a NiO layer; (3) drying the substrate by the hot air for 20 s and (4) rinsing the substrate in a separate H_2O beaker for 20 s to remove large and loosely bound NiO particles. Thus, one SILAR cycle of NiO deposition was completed. By repeating such deposition cycles for 60–150 times, we obtained the NiO film thicknesses (t) in the 420–1050 nm range. After that, NiO samples were annealed at 550 °C for 2 h in air ambient. For the doping of the deposited via SILAR nickel oxide films with lithium ions to obtain NiO:Li layers, the glass substrates immediately after their covering by NiO films were immersed into saturated aqueous solution of lithium hydroxide (LiOH) and held there at room temperature for 20 min. After that, NiO:Li samples were annealed at 550 °C for 2 h in air ambient.

The morphology of the NiO and NiO:Li films was observed by scanning electron microscopy (SEM) in secondary electron mode. The SEM instruments (JEOL JSM-840 and Tescan Vega 3 LMH) were operated at an accelerating voltage of 20 kV (JSM-840) and 30 kV (Vega 3) without the use of additional conductive coatings. The NiO thickness data were obtained from SEM images of the NiO and NiO:Li films exfoliated after annealing in air ambient.

Optical properties of the NiO and NiO:Li films were studied in the wavelength (λ) range 300–1100 nm, both before and after annealing with an "SF-2000″ spectrophotometer equipped with "SFO-2000″ specular and diffuse reflection attachment. To study the optical properties, the unnecessary NiO and NiO:Li films were removed from one side of the glass substrate by rubbing with concentrated HCl acid. Uncoated glass substrates were used as control samples when optical transmission spectra $T_O(\lambda)$ were recorded. Optical band gaps E_g of the NiO and NiO:Li films were determined from their absorption coefficients (α) calculated as:

$$\alpha = 1/t \cdot \ln(1/T_O) \quad (1)$$

where t is the film thickness. Then, the optical bandgaps E_g of NiO and NiO:Li were estimated by employing the Tauc model [9,23,24]:

$$(\alpha \cdot h\nu)^2 = A \cdot (h\nu - E_g), \quad (2)$$

where A is a constant and $h\nu$ denotes the photon energy. The optical band gap of the thin film was determined by extrapolating the linear section of $(\alpha \cdot h\nu)^2$ vs $h\nu$ to the energy axis.

In addition, the optical band gaps of the NiO:Li translucent and opaque films were evaluated in accordance with [8] from the Kubelka-Munk function:

$$F(R) = \frac{(1-R)^2}{2R}, \quad (3)$$

where R is the optical reflectance. As shown in [8], the plots of $(F(R) \cdot h\nu)^2$ vs $h\nu$ yield the band gap E_g values of the materials by extrapolating of their linear parts on $h\nu$.

According to [28], since the exponential dependence of absorption coefficient on incident photon energy in the Urbach region ($h\nu < E_g$) is due to the perturbation of the parabolic density of the states at the band edge, the Urbach energy (E_o) originates from the optical transitions assisted by subband gap photons. In the low photon energy range it is assumed that the spectral dependence of absorption edge follows the empirical Urbach rule is given, in accordance with [29], by equation:

$$a(\nu) = \alpha_o \cdot \exp(h\nu/E_o), \quad (4)$$

where α_o is a constant.

Urbach energy is often interpreted as the width of the tail of localized states in the band gap. So, according to [28,29], the structural disorders of the NiO and NiO:Li films were assessed by the E_o determined by fitting the linear portions of ln(α) versus hν, namely, from the slope of the linear part of the dependence ln(α) on hν near the band gap energy value.

To analyze phase compositions, structural and substructural parameters of the NiO and NiO:Li films we recorded X-ray diffraction patterns (XRD) by a DRON-4 diffractometer with Bragg–Brentano focusing (theta – 2 theta). The resulting X-ray diffraction patterns were processed and the profile parameters of the diffraction lines were calculated by "New-Profile v.3.4 (486)" and "OriginPro v.7.5″ software. The presence of crystalline phases was revealed by comparing the experimental diffraction patterns with the reference database JCPDS with the use of PCPDFWIN v.1.30 software. The sizes of the coherent-scattering domains (CSD) in NiO and NiO:Li films as well as microstrains ε were estimated by analyzing the broadening of the X-ray diffraction peaks by the method of Williamson–Hall approximations [30] or, if the number of peaks was insufficient, the sizes of NiO and NiO:Li crystallites were obtained using the X-ray diffraction data via Scherer's method [4,23].

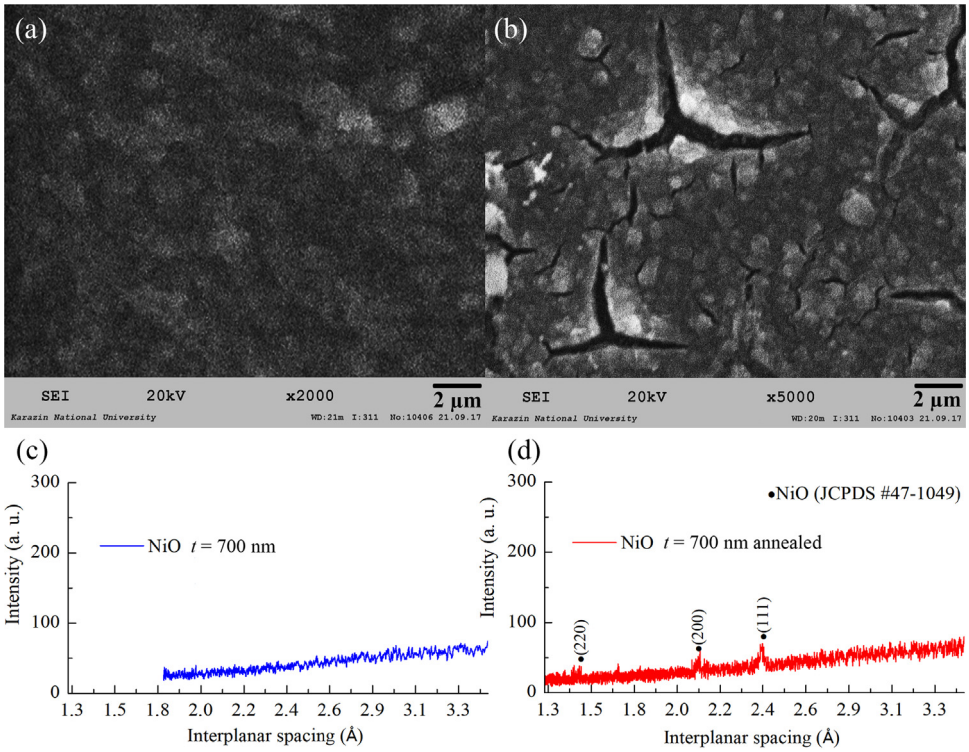

Fig. 1. Top view SEM images (a, b) and XRD patterns (c, d) of 700 nm thick NiO film as-prepared via SILAR (a, c) and annealed at 550 °C for 2 h in air ambient (b,d).

Similar to that described in [4,23,31], it was suggested that CSDs are equal to the average sizes of the nanocrystalline NiO or NiO:Li grains.

The crystal lattice parameters a were calculated from the positions of the all indexed lines in the X-ray diffraction patterns by the Nelson–Riley graphical extrapolation method [7,32]. The a value was calculated precisely using the Nelson-Riley functions (NRF) obtained by the following equation [32]:

$$NRF = 0.5\cdot\left(\frac{\cos^2\theta}{\sin\theta} + \frac{\cos^2\theta}{\theta}\right), \quad (5)$$

where θ is the Bragg angle derived from XRD pattern.

Then the calculated lattice parameters a for different θ values were plotted against Nelson-Riley function, and the extrapolation of the line to the Y-axis gave the accurate lattice parameter of the crystal system.

Texture quality of the NiO and NiO:Li films was estimated by the Harris method [8]. Pole density P_i, which determines an axis of the crystal plane that is oriented normal to the surface, was calculated according to the equation [8]:

$$P_i = (I_i/I_{0i})/[1/N\sum_{i=1}^{N}(I_i/I_{0i})], \quad (6)$$

where I_i, I_{oi} are integral intensity of the i-th diffraction peak of the film samples and etalon, respectively; N is the number of lines presented in the XRD pattern. Texture axis has the index, which corresponds to the largest value of P_i. The orientation factor f for the relevant direction was calculated from the formula:

$$f = \sqrt{1/N\sum_{i=1}^{N}(P_i - 1)^2}. \quad (7)$$

The conductivity type of the NiO and NiO:Li films was determined using the standard hot-probe method [33]. The resistivities ρ of the NiO and NiO:Li films were measured in accordance with [7] by using a four-point collinear probe resistivity method. The resistivity was calculated by the following equation:

$$\rho = (\pi t\delta U_{23})/(I_{14}\cdot \ln 2), \quad (8)$$

where δ is a correction factor based on the ratio of the distance between probes to the substrate dimensions (in our case $\pi\delta/\ln 2 = 4.45$).

The activation energies E_a of the NiO and NiO:Li films were calculated from the gradients of ln ρ vs. 10^3/T plots based on the following equation [14,34]:

$$\rho = \rho_0 \exp(E_a/kT), \quad (9)$$

where ρ is the resistivity at temperature T, ρ_0 is a constant, k is the Boltzmann constant.

The carrier concentration (n) and mobility (μ) in the NiO and NiO:Li films were characterized by a Hall effect at room temperature in accordance with [35] using a homemade Hall measurement system with a van der Pauw configuration. The comparison of the temperature-dependent resistivities of the NiO and NiO:Li films was fulfilled with the help of resistive heating of these semiconductor films within the T range 290–390 K. A homemade thermoregulated resistive heater was situated under the plate, on which the glass substrate with NiO or NiO:Li film was located. A schematic of the homemade resistance measurement system was presented in [7]. It includes a voltmeter with high input resistance, a variable resistor for regulating the operating mode of the power supply of the measuring circuit, a very sensitive electrometer, a switcher, a stabilized current source, the probe array and the thermoregulated resistive heater.

The Seebeck coefficients Z were measured in accordance with [4,17,20] as the induced thermoelectromotive forces ΔV in response to the temperature gradients ΔT along the NiO and NiO:Li films deposited on the glass substrates. In order to identify the in-plane Seebeck coefficients we used homemade measurement setup described in [7]. Temperature gradient was produced by means of the Peltier unit TEC1–12730, which was connected to the independent temperature controller, and was applied along the film sample and measured using a pair of chromel-alumel thermocouples. By plotting the measured thermoelectromotive force ΔV vs the applied temperature gradient ΔT, the Z value was determined as a slope of the branch obtained at the near room temperature range 290–390 K. Then, the thermoelectric power factors P for the the NiO and NiO:Li films were calculated, in

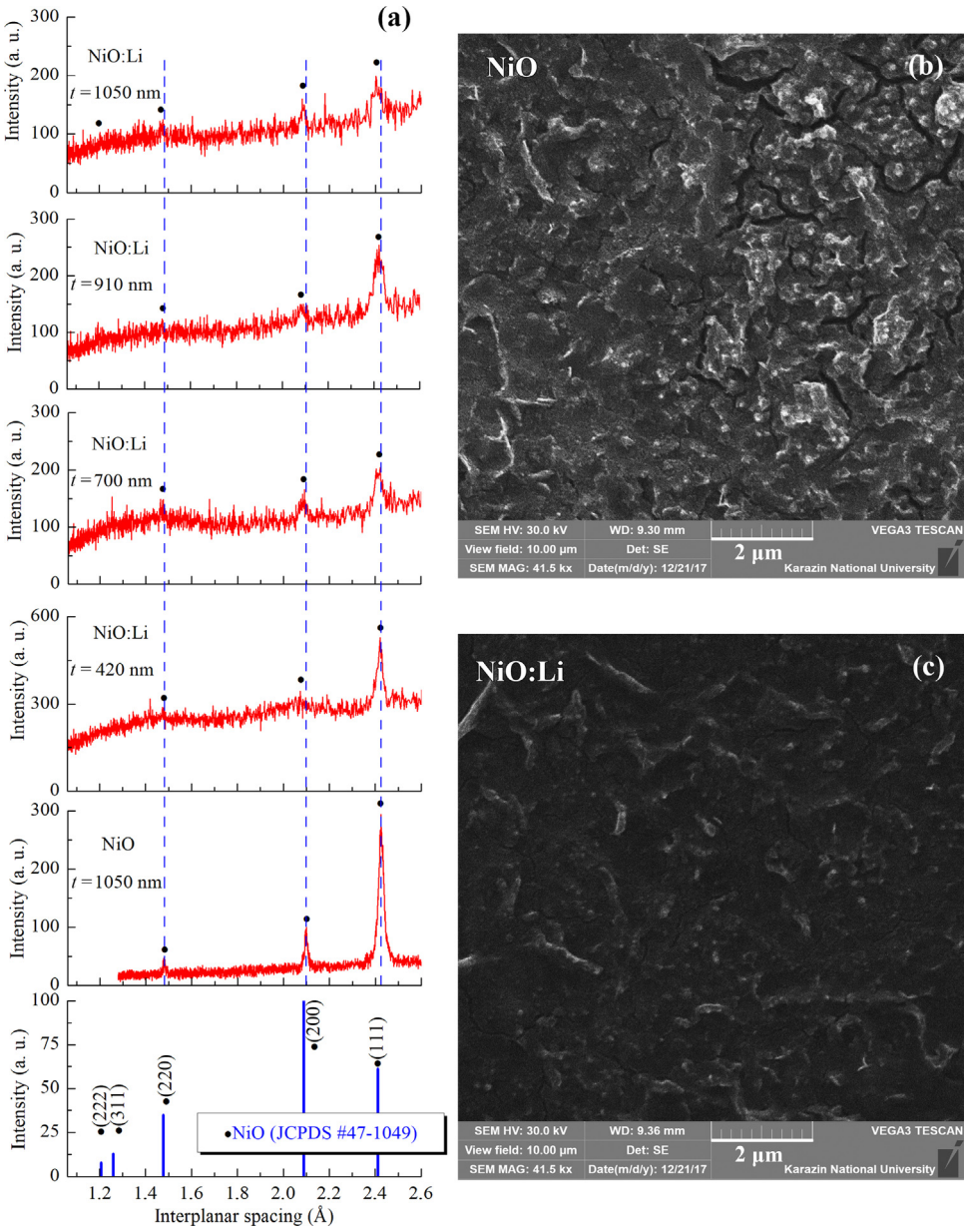

Fig. 2. XRD patterns of the prepared via SILAR 1050 nm thick NiO film after its annealing and of the NiO:Li films of different thicknesses after their processing in LiOH solution and annealing (*t* values equal 420 nm, 700 nm, 910 nm and 1050 nm) (a). Top view SEM images of 420]nm thick NiO (b) and NiO:Li (c) films.

accordance with [17,19], as $P = Z^2/\rho$.

3. Results and discussions

Fig. 1 presents structure of the as-deposited via SILAR NiO film (a,c) and this film after annealing in air (b,d). As seen, NiO film immediately after deposition is smooth and amorphous, but its annealing in air promotes recrystallization, which, however, is accompanied by the appearance of deep cracks throughout the NiO film thickness. As can be seen from the comparison of structure of the annealed nickel oxide films with different thicknesses in Figs. 1(b,d) and 2(a,b), the observed XRD-peaks correspond to the (111), (200) and (220) planes of the cubic rock-salt NiO structure with a space group of fm3m (JCPDS # 47-1049). The SEM images in Fig. 1(b) and (b) demonstrate cracks, which abundance increases with NiO thickness. The crystallization of the SILAR-produced nickel oxide films after annealing in air with their cracking was noted early by [15], and this was qualitatively confirmed additionally in [15] by the surface appearance changing, that we also observe in the photos in Fig. 3. In accordance with [36], the annealing of NiO films in air possesses the tendency to form the metal-deficient NiO films with high concentration of nickel vacancies (V_{Ni}) due to the low formation energy of V_{Ni}. Upon formation of the Ni vacancy, two holes are released that transform two nearby Ni^{2+} into Ni^{3+}, and thus, lead to a local distortion of the lattice. As confirmation, the microstresses ($\varepsilon = \Delta d/d$, where d is the crystal interplanar spacing according to JCPDS, and Δd is the difference between the experimental and reference interplanar spacings) in the obtained in our work NiO films after their annealing in air are quite large, namely $1.1{\cdot}10^{-2}$ and $6{\cdot}10^{-3}$ a. u., for 700 nm and 1050 nm thick NiO films, correspondingly (Table 1).

As can be seen in Figs. 1(d) and 2(a), the intensity of the NiO XRD-peaks increased regularly with NiO thickness. However, calculations of the NiO grain sizes using Scherer's formula have shown that the average grain size is slightly increased with NiO thickness, remaining within 10–18 nm (Table 1). Such grain sizes for the annealed NiO films obtained via SILAR method coincide with data [25] about the average grain size of NiO ~13 nm after annealing in air at 575 °C for 2 h. It can

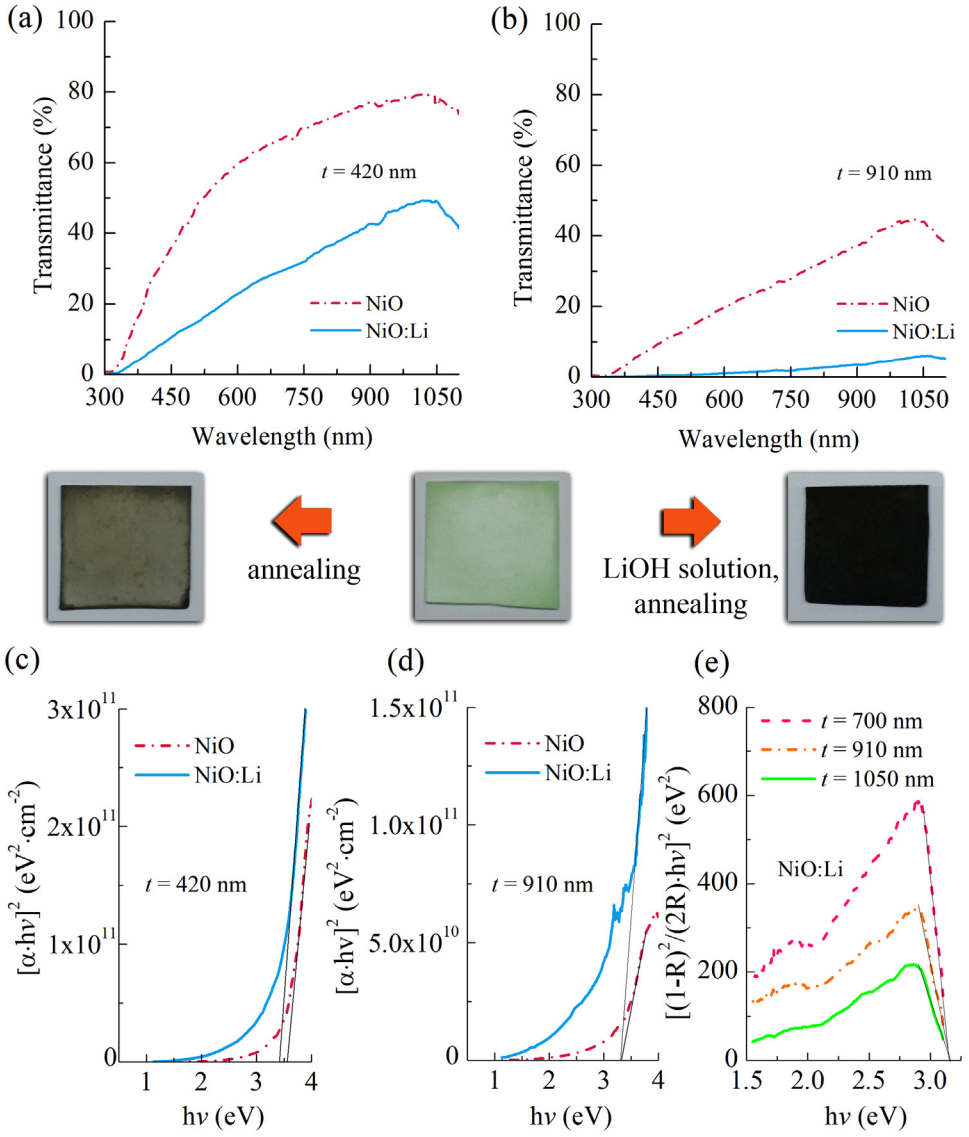

Fig. 3. Optical properties of the prepared via SILAR NiO films after their annealing and of the NiO:Li films after their processing in LiOH solution and annealing: (a, b) – transmittance spectra; (c, d) – graphs for the determination E_g according to Eq. (2); (e) – graphs for the determination E_g according to Eq. (3). The photos of changes in the appearance of the 700 nm thick NiO film after its annealing and of the 700 nm thick NiO:Li film after its processing in LiOH solution and following annealing.

Table 1
Structural parameters of NiO and NiO:Li films of different thicknesses *t*.

Sample	Thickness *t*, nm	Grain size (CSD), nm	Microstrains $\Delta d/d$, 10^{-3} a. u.
NiO	700	10	11.0
NiO:Li		11–15	8.2–9.7
NiO	910	16	7.0
NiO:Li		11–13	7.9–12.0
NiO	1050	18	6.0
NiO:Li		11–15	1.1–3.5

be seen from Fig. 2(a) that all diffraction peaks of the NiO:Li films belong to NiO, but the interplanar distances corresponding to these peaks are slightly shifted to lesser *d* values. The XRD spectra of the NiO:Li films of different thickness show (Fig. 2(a)) a decrease in the intensity of the XRD peaks due to a diminution in the degree of crystallinity of NiO phase without the appearance of any impurity phases. All the above leads to the conclusion, that these NiO:Li samples are single phased Li-NiO solid solutions. Table 1 presents data, which demonstrate a slight decrease in the sizes of nanograins, which dimensions are 11–15 nm, and quite large microstrains in the lithium-doped nickel oxide films. Such microstrains connected with the doping of nickel oxide with lithium, which results in acute lattice distortion, were observed in [17]. As shown by calculations, the most thick NiO:Li film (t = 1050 nm) is very slightly preferentially oriented along < 111 > direction, its orientation factor for (111) plane is f = 0.6. According to the calculations by the Nelson–Riley graphical extrapolation method [7,32], the NiO:Li films are characterized by minor decrease in the lattice parameters a of the cubic phase of NiO, the obtained for the 1050 nm thick NiO:Li film a = 4.177 Å. In accordance with [20], such reduction of the lattice constant corresponds to ~1 at% Li. As noted in [17,20,24], the shifting of diffractions is related with the substitution of Li^+ for Ni^{2+}, as Li^+ and Ni^{2+} have the same coordination numbers and the ionic radii are 0.69 and 0.76 Å, respectively. According to [17,20], as radius of Li^+ ion is 5% smaller than that of Ni^{2+}, the substitution of Li^+ for Ni^{2+} will cause a reduction of the lattice constant. As it seen in Fig. 2(a), all XRD peaks of NiO:Li films are shifted a little, so, Li^+ replaces Ni^{2+} on all lattice planes randomly and there is no anisotropy, in other words, lithium ions distribute uniformly in the lattice of NiO. As indicated in [17], the uniform distribution of Li^+ results in the isotropy

of thermoelectric properties of NiO: Li, which is significant for excellent thermoelectric materials.

Top view SEM image of 420 nm thick NiO:Li film in Fig. 2(c) demonstrates, that the film uniformly covers the surface of the glass substrate and almost does not contain cracks, that is also very important for the use in thermoelectric devices.

According to investigation of the NiO and NiO:Li optical properties, which results are presented in Fig. 3, the lithium doping significantly reduces the transparency of the films (Fig. 3(a,b), dark film in the photo). The 910–1050 nm thick NiO:Li films are black and almost completely opaque. It can be seen from the dependences in Fig. 3(c,d), that the decrease of E_g from 3.3 to 3.6 eV for NiO films to 3.3–3.4 eV for NiO:Li ones due to the lithium doping is accompanied by a broadening of Urbach's tail, that is, by the creation of a large number of localized states in the band gap. The results of determining the E_g using the Kubelka-Munk function shown in Fig. 3(e) roughly correspond to the data obtained by the Eq. (2) for 420–910 nm thick NiO:Li films, and give value E_g = 3.2 eV as for almost opaque NiO:Li film with t = 1050 nm. As have shown by the calculations of the Urbach's energy, E_o increases up to 2.1–2.2 eV due to the Li-doping and with the NiO:Li film thickness. Such large values of the Urbach's energy indicate disordering in the NiO:Li structure related to additional defects caused by doping.

Studies with the use the hot-probe method showed that all obtained NiO and NiO:Li films have p-type of conductivity. Fig. 4(a) presents data about resistivities of the NiO and NiO:Li films were measured at the temperatures T in the 290–390 K range by using the four-probe method. Note that the resistance measuring for the NiO films was accompanied by difficulties, which, probably, associated with the presence of cracks. So, Fig. 4 shows data for only one NiO film with t = 1050 nm. Nevertheless, the obtained for the deposited via SILAR and annealed in air ambient NiO film resistivity values are much less than ρ for ceramics based on polycrystalline nickel oxide in [17] or of the same order of magnitude as ρ in [19]. Our undoped nickel oxide film has resistivity equal to NiO thin layers grown by sputtering at various temperatures in pure Ar and O_2 atmospheres in [12], and about two orders of magnitude smaller ρ, than values for the NiO films fabricated in [21] by sol-gel method, and also about 3–5 orders of magnitude smaller, than ρ of NiO films obtained by chemical bath deposition in [9].

Since in accordance with [13], the most important defect in pristine p-NiO is the Ni vacancy (V_{Ni}), and other intrinsic defects: O vacancy (V_O), Ni interstitial (Ni_i) and O interstitial (O_i), have a high formation energy (above 2 eV), then, V_{Ni} is the cause of nonstoichiometry in NiO as the predominating point defect defining NiO electrical properties, that is confirmed by other authors [16,24,36,37]. The rather low electrical conductivity of pure NiO films is associated [13,37] with comparatively large ionization energy of the Ni vacancy.

It is shown in Fig. 4(a), that treatment in LiOH solution before annealing of NiO films with their transformation into NiO:Li significantly reduces ρ values, because, in accordance with [20], the substitution of Li^+ for Ni^{2+} increase the concentration and mobility of the carriers. According to our measurements of the Hall effect, the obtained 1050 nm thick NiO film has $n \approx 1.1 \times 10^{13}$cm^{-3}, μ ≈ 7 cm^2/V s, and NiO:Li film of the same thickness is characterized by the values $n \approx 1.2 \times 10^{16}$ cm^{-3}, μ ≈ 10 cm^2/V s. Since the process of Li-doping is realized through the surface of the nickel oxide, the smallest effect of lithium doping is observed in Fig. 4(a) for the most thick NiO:Li film (t = 1050 nm). All NiO and NiO:Li films show semiconducting behavior. So, as it explained in [13,20,24], when Li^+ ions are introduced in the nickel oxide film as dopant, Li^+ goes into the substitutional sites of Ni^{2+} and traps electron and generates excess of uncompensated holes due to shallow Li_{Ni} defects.

As calculations of the activation energy on the base of data presented in Fig. 4(b) have shown, all solution-processed Li-doped NiO films grown by SILAR have similar E_a values 0.25–0.31 eV. Although activation energy of our undoped NiO film equals only 0.1 eV, this film is less conductive, apparently due to lower carrier concentration in NiO in comparison with NiO: Li. According to [24,37,38], V_{Ni} and Li_{Ni} defects have close values of their formation enthalpies, so, the carriers in both, the doped and the undoped films are the same localized holes present at the Ni^{3+} centers, and the activation energy in conductivity measurements is associated with the thermally activated mobility.

Fig. 5(a) shows variation of the thermoelectromotive forces ΔV at near room temperatures with gradients ΔT along the NiO:Li films of different thicknesses. The obtained in-plane Seebeck coefficients Z are in the range 0.20–0.33 mV/K, that is, the Z correspond to the data for the thermoelectric Li-doped NiO ceramics [17,19,20].

As it seen in Fig. 5(a), the 700 nm thick solution-processed Li-doped NiO films grown by SILAR on glass substrate can generate 25 mV of voltage, when subjected to around 75 K temperature difference through a heating of one end to as low as 95 °C and a maintaining the other end at room temperature (20 °C).

The dependence of thermoelectric power factors P on the temperature shown in Fig. 5(b) has a shape typical for thermoelectric materials. Notwithstanding the fact that the characteristic for lithium-doped NiO ceramics [17] maximum values of P = 2.2 μW/K^2·m, are rather small, they were achieved in this work when the hot end of the NiO:Li film was heated only to 115 °C. Thus, in this work we succeeded

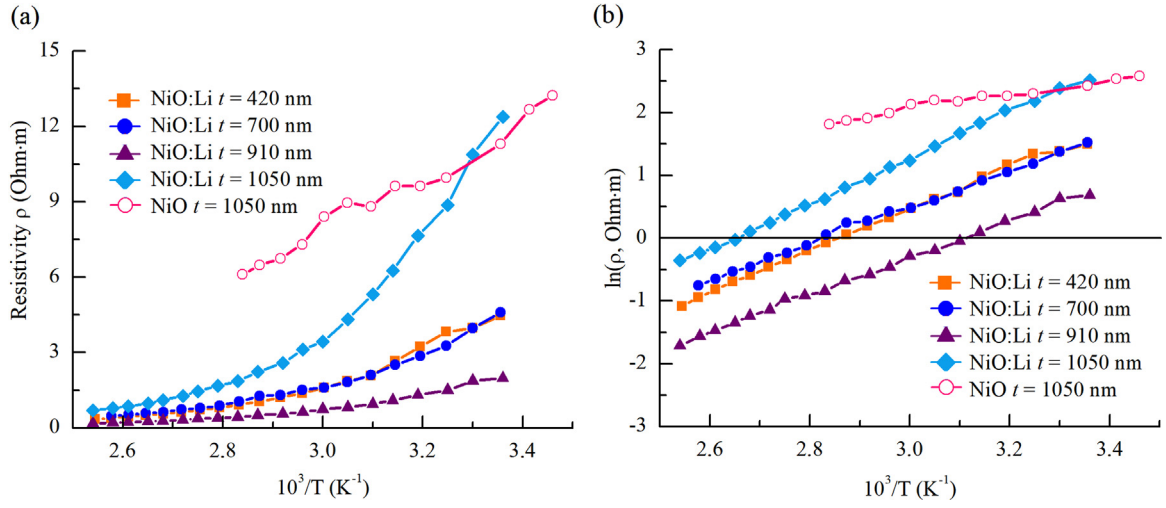

Fig. 4. Temperature dependences of the electrical resistivity ρ (a) and ln ρ (b) for the prepared via SILAR NiO film after its annealing and for the NiO:Li films of different thicknesses after their processing in LiOH solution and annealing.

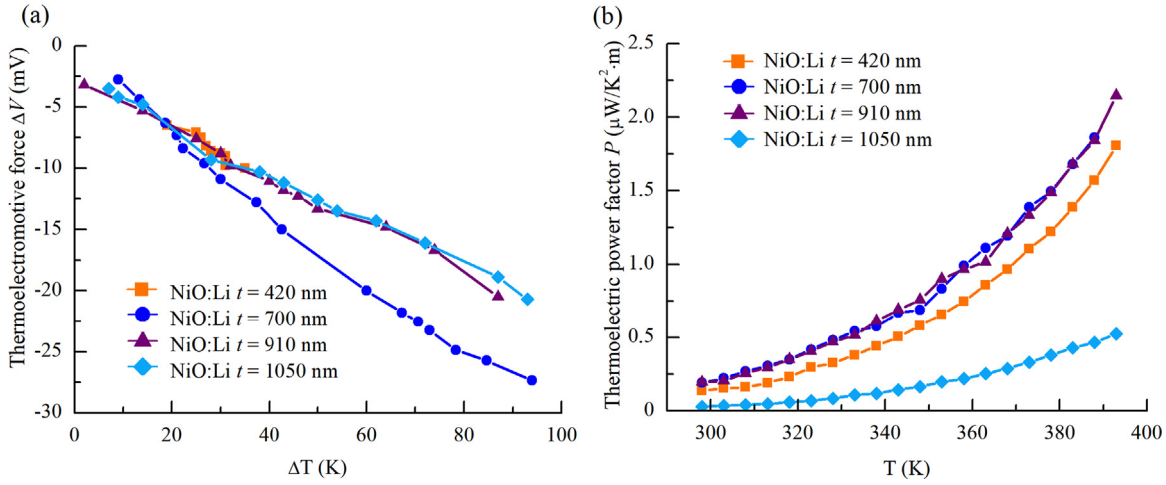

Fig. 5. Variation of the thermoelectromotive forces ΔV in response to the temperature gradients ΔT along the NiO:Li films (a) and temperature dependences of the thermoelectric power factors P (b) for the prepared via SILAR NiO:Li films of different thicknesses after their processing in LiOH solution and annealing.

to fabricate new low cost thermoelectric thin film material suitable for a production of electrical energy for low-power devices due to absorption of low-potential heat.

4. Conclusions

In this paper we present the results of the development the new low temperature solution growth method for a creating thin-film non-poisonous, earth-abundant, inexpensive and stable thermoelectric material Li-doped NiO, which can effectively utilize low temperature heat with micro-Watts electrical power output at temperature differences of several tens of Kelvins. The facial synthesis of the NiO:Li films is based on the Successive Ionic Layer Adsorption and Reaction with the processing of the obtained NiO films in a lithium-containing aqueous solution for their transformation after annealing into NiO:Li layers. Comparative analysis of crystal structure, optical, electrical and thermoelectric properties of the obtained NiO and NiO:Li 420–1050 nm thick films have reveiled a cubic rock-salt NiO structure with a space group of fm3m, at that, NiO:Li samples are nanocrystalline single phased Li-NiO solid solutions. The NiO:Li films are homogeneous, free of cracks and dark in appearance because of the large number of Li_{Ni} defects in the band gap, which significantly reduce electrical resistivity of the films, since Li^+ ions substitute Ni^{2+} and generate excess of uncompensated holes. The fabricated NiO and NiO:Li films are *p*-type semiconductors with activation energy E_a = 0.1 eV and E_a = 0.25–0.31 eV, respectively. The obtained in-plane Seebeck coefficients Z are in the range 0.20–0.33 mV/K. Notwithstanding the fact that the maximum values of the thermoelectric power factors P = 2.2 μW/K^2 m, are rather small, they were achieved if the hot end of the NiO:Li film was heated only to 115 °C.

Conflicts of interest

The authors declare no competing interest.

References

[1] M.T. Dunham, M.T. Barako, S. LeBlanc, M. Asheghi, B. Chen, K.E. Goodson, Power density optimization for micro thermoelectric generators, Energy 93 (2015) 2006–2017, http://dx.doi.org/10.1016/j.energy.2015.10.032.
[2] Y. Wu, Z. Lin, Z. Tian, C. Han, J. Liu, H. Zhang, Z. Zhang, Z. Wang, L. Dai, Y. Cao, Z. Hu, Fabrication of microstructured thermoelectric Bi_2Te_3 thin films by seed layer assisted electrodeposition, Mater. Sci. Semicond. Process. 46 (2016) 17–22, http://dx.doi.org/10.1016/j.mssp.2016.01.014.
[3] M. Hyland, H. Hunter, J. Liu, E. Veety, D. Vashaee, Wearable thermoelectric generators for human body heat harvesting, Appl. Energy 182 (2016) 518–524, http://dx.doi.org/10.1016/j.apenergy.2016.08.150.
[4] E.A. Mondarte, V. Copa, A. Tuico, C.J. Vergara, E. Estacio, A. Salvador, A. Somintac, Al-doped ZnO and N-doped Cu_xO thermoelectric thin films for self- powering integrated devices, Mater. Sci. Semicond. Process. 45 (2016) 27–31, http://dx.doi.org/10.1016/j.mssp.2016.01.013.
[5] C. Yang, D. Souchay, M. Knei, M. Bogner, H.M. Wei, M. Lorenz, O. Oeckler, G. Benstetter, Y.Q. Fu, M. Grundmann, Transparent flexible thermoelectric material based on non-toxic earth-abundant p-type copper iodide thin film, Nat. Commun. 8 (2017) 16076-1–16076-7, http://dx.doi.org/10.1038/ncomms16076.
[6] C. Han, Q. Sun, Z. Li, S.X. Dou, Thermoelectric enhancement of different kinds of metal chalcogenides, Adv. Energy Mater. 6 (2016) 1600498-1–1600498-36, http://dx.doi.org/10.1002/aenm.201600498.
[7] N.P. Klochko, V.R. Kopach, I.I. Tyukhov, G.S. Khrypunov, V.E. Korsun, V.O. Nikitin, V.M. Lyubov, M.V. Kirichenko, O.N. Otchenashko, D.O. Zhadan, M.O. Maslak, A.L. Khrypunova, Wet chemical synthesis of nanostructured semiconductor layers for thin-film solar thermoelectric generator, Sol. Energy 157 (2017) 657–666, http://dx.doi.org/10.1016/j.solener.2017.08.060.
[8] S.K. Kuanr, G. Vinothkumar, K.S. Babu, Substrate temperature dependent structural orientation of EBPVD deposited NiO films and its influence on optical, electrical property, Mater. Sci. Semicond. Process. 75 (2018) 26–30, http://dx.doi.org/10.1016/j.mssp.2017.11.013.
[9] M. Martínez-Gil, M.I. Pintor-Monroy, M. Cota-Leal, D. Cabrera-German, A. Garzon-Fontecha, M.A. Quevedo-López, M. Sotelo-Lerma, Influence of annealing temperature on nickel oxide thin films grown by chemical bath deposition, Mater. Sci. Semicond. Process. 72 (2017) 37–45, http://dx.doi.org/10.1016/j.mssp.2017.09.021.
[10] J.-H. Oh, S.Y. Hwang, Y.D. Kim, J.-H. Song, T.-Y. Seong, Effect of different sputtering gas mixtures on the structural, electrical, and optical properties of p-type NiO thin films, Mater. Sci. Semicond. Process. 16 (2013) 1346–1351, http://dx.doi.org/10.1016/j.mssp.2012.11.003.
[11] H. Ohta, M. Hirano, K. Nakahara, H. Maruta, T. Tanabe, M. Kamiya, T. Kamiya, H. Hosono, Fabrication and photoresponse of a pn-heterojunction diode composed of transparent oxide semiconductors, p-NiO and n-ZnO, Appl. Phys. Lett. 83 (2003) 1029–1031, http://dx.doi.org/10.1063/1.1598624.
[12] Y.H. Kwon, S.H. Chun, J.-H. Han, H.K. Cho, Correlation between electrical properties and point defects in NiO thin films, Met. Mater. Int. 18 (2012) 1003–1007 (doi: 110.1007/s12540-012-6012-5).
[13] J. Osorio-Guillén, S. Lany, A. Zunger, Nonstoichiometry and hole doping in NiO, AIP Confer. Proc. 1199 (2010) 128–129, http://dx.doi.org/10.1063/1.3295330.
[14] A. Hakim, J. Hossain, K.A. Khan, Temperature effect on the electrical properties of undoped NiO thin films, Renew. Energy 34 (2009) 2625–2629, http://dx.doi.org/10.1016/j.renene.2009.05.014.
[15] S.U. Mutkule, S.T. Navale, V.V. Jadhav, S.B. Ambade, M. Naushad, A.D. Sagar, V.B. Patil, F.J. Stadler, R.S. Mane, Solution-processed nickel oxide films and their liquefied petroleum gas sensing activity, J. Alloy. Compd. 695 (2017) 2008–2015, http://dx.doi.org/10.1016/j.jallcom.2016.11.037.
[16] W.-L. Jang, Y.-M. Lu, W.-S. Hwang, W.-C. Chen, Electrical properties of Li-doped NiO films, J. Eur. Ceram. Soc. 30 (2010) 503–508, http://dx.doi.org/10.1016/j.jeurceramsoc.2009.05.041.
[17] Y. Lu, L. Hao, H. Yoshida, M. Hirohashi, Reaction behaviour of $Ni_{1-x}M_xO$'s (M = Li, Na) formation and its thermoelectric properties, J. Mater. Sci: Mater. Electron 23 (2012) 315–319, http://dx.doi.org/10.1007/s10854-011-0411-0.
[18] P.L. Bach, J.M. Vila-Fungueiriño, V. Leborán, E. Ferreiro-Vila, B. Rodríguez-González, F. Rivadulla, Strain-induced enhancement of the thermoelectric power in thin films of hole-doped $La_2NiO_{4+\delta}$, APL Mater. 1 (2013) 021101-1–021101-6, http://dx.doi.org/10.1063/1.4818356.
[19] W. Shin, N. Murayama, High performance p-type thermoelectric oxide based on NiO, Mater. Lett. 45 (2000) 302–306, http://dx.doi.org/10.1016/S0167-577X(00)00122-1.
[20] S. Liu, J. Wang, J. Jia, X. Hu, S. Liu, Synthesis and thermoelectric performance of Li-

doped NiO ceramics, Ceram. Int. 38 (2012) 5023–5026, http://dx.doi.org/10.1016/j.ceramint.2012.02.099.
[21] W. Guo, K.N. Hui, K.S. Hui, High conductivity nickel oxide thin films by a facile sol–gel method, Mater. Lett. 92 (2013) 291–295, http://dx.doi.org/10.1016/j.matlet.2012.10.109.
[22] C.-H. Han, S.-D. Han, I. Singh, Thermoelectric hydrogen sensor using $Li_xNi_{1-x}O$ synthesized by molten salt method, Korean J. Chem. Eng. 23 (2006) 362–366, http://dx.doi.org/10.1007/BF02706735.
[23] I. Sta, M. Jlassi, M. Kandyla, M. Hajji, P. Koralli, R. Allagui, M. Kompitsas, H. Ezzaouia, Hydrogen sensing by sol–gel grown NiO and NiO:Li thin films, J. Alloy. Compd. 626 (2015) 87–92, http://dx.doi.org/10.1016/j.jallcom.2014.11.151.
[24] T. Dutta, P. Gupta, A. Gupta, J. Narayan, Effect of Li doping in NiO thin films on its transparent and conducting properties and its application in heteroepitaxial p-n junctions, J. Appl. Phys. 108 (2010) 083715-1–083715-7, http://dx.doi.org/10.1063/1.3499276.
[25] T. Taşköprü, F. Bayansal, B. Şahin, M. Zor, Structural and optical properties of Co-doped NiO films prepared by SILAR method, Philos. Mag. 95 (2015) 32–40, http://dx.doi.org/10.1080/14786435.2014.984788.
[26] Y. Akaltun, T. Çayır, Fabrication and characterization of NiO thin films prepared by SILAR method, J. Alloy. Compd. 625 (2015) 144–148, http://dx.doi.org/10.1016/j.jallcom.2014.10.194.
[27] D. Lee, Q.X. Xia, R.S. Mane, J.M. Yun, K.H. Kim, Direct successive ionic layer adsorption and reaction (SILAR) synthesis of nickel and cobalt hydroxide composites for supercapacitor applications, J. Alloy. Compd. 722 (2017) 809–817, http://dx.doi.org/10.1016/j.jallcom.2017.06.170.
[28] M. Tyagi, M. Tomar, V. Gupta, Optical properties of NiO thin films: a potential material for optoelectronic devices, Adv. Mater. Res. 488–489 (2012) 103–108, http://dx.doi.org/10.4028/www.scientific.net/AMR.488-489.103.
[29] M.O. Dawood, Effect of Cu-doping on Urbach Energy and dispersion parameters of Cu: NiO film deposited by CSP, Int. Lett. Chem. Phys. Astron. 48 (2015), pp. 138–145, http://dx.doi.org/10.18052/www.scipress.com/ILCPA.48.138.
[30] A.K. Zak, W.H.A. Majid, M.E. Abrishami, R. Yousefi, X-ray analysis of ZnO nanoparticles by Williamson–Hall and size–strain plot methods, Solid State Sci. 13 (2011) 251–256, http://dx.doi.org/10.1016/j.solidstatesciences.2010.11.024.
[31] T. Ungár, G. Tichy, J. Gubicza, R.J. Hellmig, Correlation between subgrains and coherently scattering domains, Powder Diffr. 20 (2005) 366–375, http://dx.doi.org/10.1154/1.2135313.
[32] A.K. Soman, P. Kuppusami, A.M. Rabel, Electrical conductivity of NiO-gadolinia doped ceria anode material for intermediate temperature solid oxide fuel cells, Nano Hybrids Compos. 17 (2017) 224–236, http://dx.doi.org/10.4028/www.scientific.net/NHC.17.224.
[33] A. Axelevitch, G. Golan, Hot-probe method for evaluation of majority charged carriers concentration in semiconductor thin films, Facta Univ. Ser.: Electron. Energy 26 (2013) 187–195, http://dx.doi.org/10.2298/FUEE1303187a.
[34] U.J. Chavan, A.A. Yadav, Structural, optical and electrical properties of chemical bath deposited NiO thin films, Int. J. Eng. Sci. Res. Technol. 5 (2016) 282–287, http://dx.doi.org/10.5281/zenodo.160859.
[35] F. Werner, Hall measurements on low-mobility thin films, J. Appl. Phys. 122 (2017) 135306-1–135306-14, http://dx.doi.org/10.1063/1.4990470.
[36] R. Karsthof, P. Räcke, H. von Wenckstern, M. Grundmann, Semi-transparent NiO/ZnO UV photovoltaic cells, Phys. Status Solidi A 213 (2016) 30–37, http://dx.doi.org/10.1002/pssa.201532625.
[37] H.J. Van Daal, A.J. Bosman, Influence of native defects on transport properties of Li-doped NiO, Phys. Lett. 23 (1966) 525–526, http://dx.doi.org/10.1016/0031-9163(66)90389-1.
[38] J.A. Dawson, Y. Guo, J. Robertson, Energetics of intrinsic defects in NiO and the consequences for its resistive random access memory performance, Appl. Phys. Lett. 107 (2015) 122110-1–122110-5, http://dx.doi.org/10.1063/1.4931751.